Technical note : Generation of tissue folds by oriented cells in a coupled von Karman–tensor model and application to biometrics

Vincent Fleury, Maël Berthier

Technical note : Generation of tissue folds by oriented cells in a coupled von Karman-Q-tensor model and application to biometrics

Vincent Fleury[1,2] and Maël Berthier[2]

[1]Laboratoire Matière et Systèmes Complexes, Université de Paris-Cité/CNRS

10 rue Alice Domont et Léonie Duquet 750013 Paris, France

[2]on leave from Idemia, 52 Chaussée Jules César 95520 Osny, France

Abstract

Biophysics of development is progressing steadily. It is recognized that formation of organs is a biomechanical process including stresses and deformations. From a theoretical point of view, it is necessary to include forces in tissue development to understand how forms unfold. However, living tissue is not a uniform material, it is composed of cells, and cells tend to form organized layers. We present a theoretical framework which is able to produce biological forms from a plate theory coupled to an active nematoïd field. The theory consists of a von Karman plate equation coupled to a Q-tensor dynamics, however, in this description the Q-tensor is not a static description of a nematoïd field but the actuator of a field of force. The Q-tensor serves as active stress in the von Karman equation to generate thin plate out-of-plane deformations (buckling). A simple application of this model is presented: the formation of fingerprints. The model is able to easily produce fingerprints, including potentially actual fingerprints.

In recent years, mechanical features have been invoked in many if not all biological processes. In developmental biology, visco-elastic movements have been invoked for the description of many phases of embryo development. Especially, the embryonic body forms by a deterministic folding process (1), and tissue folding requires mechanical stress. Cells exert stresses by several means, however traction forces are most generally exerted by actin-myosin contraction (2), which is akin to muscular contraction (3). The force exerted by cells has a magnitude which is very much variable, as evidenced for example in electric stimulation of development (4), which is able to increase developmental forces by large factors, albeit transiently (this is due to the fact that the forces exerted by cells are sensitive to potential, because ionic channels are voltage-dependent gates). Forces become significant when cells cooperate to cause stronger tractions. This occurs typically when cells align and form belts or rings of cells which behave as purse-strings (5). It has been shown

that these purse strings can exert cooperative forces of the order of 10^{-6} N (5). Such purse strings are ubiquitous in embryo development: rings of aligned or stacked cells fold the surface and generate pits such as otic or nasal pits (6). Even in organ development, such as gut development, cells self-organize in rings around the tubes (7, 8). Therefore, from a mechanical point of view, tissues are not homogeneous, they consist of cells which have a tendency to self-organize in a nematoïd order (9). In addition, this order is itself influenced by such cues as surface curvature (8). In return, organized cells exert stronger forces, which are able to generate curvature (5).

In physics, the formation of a nematoïd order with local parameter **N** can be described by a Landau energy $(\mathbf{grad\ N})^2$(10) if both orientation and direction are important, or by a de Gennes direction-free Q-tensor (10), if orientation is important but direction is irrelevant. (This comes from the fact that in descriptions by an energy of the form $(\mathbf{Grad\ N})^2$, the gradient is maximal when there is a boundary between **+N** and **–N**, while this is nonsensical if the direction of the vector **N** does not matter (+**N** and –**N** describe the same orientation, and the energy to cross a boundary +**N**/-**N** should be zero, and not maximal).

It has been suggested for long that flexure of a thin soft plate such as an ectoderm or an epidermis can be modelled by flexure of a thin plate as in von Karman equation (10, 11). However, the idea that surface stress plays a role in epidermal ridges has been seriously challenged by biological studies of the molecular pathways. It has been shown recently that a Turing process between Wn, Bmp and EDA is one possible molecular cause of the pattern of ridges, instead of a compressive stress (12). Our purpose is not to defend the mechanical approach to volar ridge formation, but rather to propose a general technical model coupling tissue flexure and nematoïd order of cells, using skin ridges as a pedagogic example. The model works as well whether the pattern of ridges is dictated by a field of nematics or by a Turing reaction-diffusion process.

The von Karman equation for a thin plate reads, with w(x,y) the height over the surface along which (x,y) are the in-plane coordinates, F(x,y) the Airy stress function, Δ^4 the bi-laplacian operator, V(w(x,y)) a restoring energy modelling the elastic behavior of the substrate (the dermis in Kucken's model (5)), and k∂w(x,y)/∂t is the viscous drag :

$$k\partial w(x,y)/\partial t+D\Delta^4 w+F_{yy}/Rx+F_{yy}/Ry-[F,w]+\partial_w V(w)=0 \qquad \text{Equ. 1}$$

with $[F,w]=F_{xx}w_{yy}+F_{yy}w_{xx}-2F_{xy}w_{xy}$

and $1/Eh+\Delta^4 F- w_{yy}/Rx- w_{xx}/Ry+ 1/2[w,w]=0$

where h is the thickness, and D is the bending modulus, formed from the Young modulus E and the Poisson ration μ :

$$D=Eh^3/12(1-\mu^2)$$

and the restoring potential V(w) reads, with ad hoc spring parameters c, a, b and pressure p

$$V(w)=pw+cw^2/2+aw^3/3+bw^4/4$$

This potential stems from a phenomenological analysis of epidermis structure, taking into account tissue pressure, elastic deformation and inside-out asymmetry of the epidermis (in the sequel we will take V=0). This equation describes the different terms in dynamic flexure of a thin plate, under the action of an in-plane stress with principle components F_{xx} and F_{yy}, and a viscous friction. This von

Karman equation has been proposed in the context of fingerprints formation by Kücken and Newell (5). In their model, by day 11 of development, finger shrinkage causes appearance a surface stress tensor **N**, which spontaneously forms fingerprints. The principle compressive stress is a vector field which generates a pattern of singularities by Brouwer's fixed point theorem (13), and the pattern of surface buckling arises spontaneously with folds forming perpendicularly to the principle stress directions by a localized Euler buckling. In the sequel we will use a simplified von Karman equation, as we will neglect the curvature of the substrate and assume that we are folding an initially flat surface, therefore the Rx and Ry terms vanish. We also assume that the stress is exerted actively by cells, and that the active stress is stronger than the passive stress. We take in addition V(w)=0. We get a simpler form for the plate flexure:

$$k\partial w(x,y)/\partial t + D\Delta^4 w + N_{xx}d^2{}_x w + N_{yy}d^2{}_y w = 0 \qquad \text{Equ. 2}$$

In simple terms this equation models the equilibrium between the local bending of an almost flat surface (encapsulated by the bilaplacian term) and the in-plane tensional or compressive stress (which appears against the second derivative considered here as a curvature along the profile) exerted by the cells.

In Kücken and Newell's model cellular orientation is irrelevant, and the tissue is considered as uniform. Here, we suggest a model in which the actuating force in the surface is generated actively by cells. Indeed, in most developmental processes, it is seen that cells align, in form of ridges, crests, folds, and that there is a strong correlation between folding and cell orientation. In addition, cell polarity is strongly related to cytoskeleton anisotropy, which itself implies an anisotropy of traction forces, with the extreme case being muscular cells which are syncytial, and may be up to meters long.

We therefore wish to implement a model of thin plate flexure, by an active orientational field. To do so, we introduce a Q-tensor in the spirit of de Gennes (10). In our simple model the Q-tensor is in plane and characterized by its 4 values Q_{ij} defined as follows :

$$Q = n \otimes n - \tfrac{1}{2}Id \qquad \text{Equ. 3}$$

i.e. $Q = \begin{bmatrix} Q_{11} & Q_{12} \\ Q_{21} & Q_{22} \end{bmatrix}$ with $Q_{11}=n_1^2-\tfrac{1}{2}$. $Q_{12}=Q_{21}=n_1n_2$ $Q_{22}=n_2^2-\tfrac{1}{2}$. or $Q_{ij}=n_in_j-\delta_{ij}/2$

The vector (n_1,n_2) is one of the eigenvectors with eigenvalue ½.

The Q-tensor implies in principle a general energy containing all module gradient, splay, bending and twist in 3D expressed as (the energy stems from the work of assembling a spatial configuration of Q-tensor) :

$$F = \sum_{\substack{i=1,2,3\\ j=1,2,3\\ k=1,2,3}} \left[\frac{L_1}{2}\left(\frac{\partial Q_{ij}}{\partial x_k}\right)^2 + \frac{L_2}{2}\frac{\partial Q_{ij}}{\partial x_i}\frac{\partial Q_{ik}}{\partial x_k} + \frac{L_3}{2}\frac{\partial Q_{ik}}{\partial x_i}\frac{\partial Q_{ij}}{\partial x_k}\right] + \sum_{\substack{i=1,2,3\\ j=1,2,3\\ k=1,2,3\\ l=1,2,3}} \left[\frac{L_4}{2} e_{lik}\, Q_{lj}\frac{\partial Q_{ij}}{\partial x_k} + \frac{L_6}{2} Q_{lk}\frac{\partial Q_{ij}}{\partial x_l}\frac{\partial Q_{ij}}{\partial x_k}\right]$$

Equ. 4

For our pedagogic purpose we will treat only the gradient term, and remain entirely in 2D, the surface being considered as almost flat :

$$F = \sum_{\substack{i=1,2\\ j=1,2\\ k=1,2}} \left[\frac{L}{2}\left(\frac{\partial Q_{ij}}{\partial x_k}\right)^2\right]$$

The spreading equations are derived by functional variation as :

$$\partial n_i/\partial t = \delta F/\delta n_i \qquad \text{Equ. 5}$$

We use the rule $\delta F/\delta n_i = \delta F/\delta Q_{jk} \cdot \partial Q_{jk}/\partial n_i$ and $\partial Q_{jk}/\partial n_i = (n_j\delta_{ki} + n_k\delta_{ji})$. After some algebra we find :

$$\partial n_1/\partial t = \delta F/\delta n_1 = L\Delta Q_{11} n_1 + L\Delta Q_{22} n_2 + 1/2 L\Delta Q_{12} n_2 \qquad \text{Equ. 6}$$

$$\partial n_2/\partial t = \delta F/\delta n_2 = L\Delta Q_{22} n_2 + L\Delta Q_{22} n_1 + 1/2 L\Delta Q_{12} n_1 \qquad \text{Equ. 6bis}$$

In which Δ is the Laplacian operator. The boundary conditions can be chosen at will. For our purpose we will choose a value of **n** aligned along the boundary along the top part of the finger and at the last finger joint, and perpendicular to the finger along the shaft of the phalanx (as observed anatomically, Fig. 1B, please see your fingers).

Now, we assume that the oriented cells actually exert a force in-plane which is congruent with the principle axis of the Q-tensor, therefore, the principle stress axis of the stress **N** in the von Karman equation will be $Q_{//}$ and $Q_{\perp}$, were $Q_{//}$ and $Q_{\perp}$ are the principle stresses in the diagonal frame of the Q-tensor, one of the vectors being (n_1, n_2), with stress magnitudes $\lambda_{//}$ and $\lambda_{\perp}$ with $\lambda_{//}$ being the higher of the two in magnitude, as we assume cells to exert stronger forces in the direction of their long axis. If we assume a contraction along the long axis $\lambda_{//}$ will be higher than $\lambda_{\perp}$ and positive.

Now, turning to von Karman equation, we insert the **N** tensor by considering it as diagonal along the principle axis of Q, with $\lambda_{//}$ and $\lambda_{\perp}$ as $N_{//}$ and $N_{\perp}$ (the eigenvalues of **N** in the diagonal frame, are the stresses exerted by cells). Locally the eigenvectors of the tensor need not be aligned with the surface principle curvatures. We therefore have a "turning" term $\Re$ which follows the orientation of the Q-tensor in the frame where it is diagonal, so

that locally the stresses are exerted along two orthogonal axes of the flexed surface, which follow the pattern of the eigenvectors (Fig. 1), and correspond to two terms of the Laplace force. This is why we need to introduce a rotation $\Re$ for the calculation of the stress term in the frame of the principle axis of stress (following also Ref. 14). The force applied on the shell is the divergence of the said stresses (we assume the magnitude of the parallel and normal stresses exerted by cells to be constant, and the force is the derivative of the two stresses acting along two curved directions of the surface profile). This gives the following equation for the variation of the surface height w :

$$k\partial w(x,y)/\partial t+D\Delta^4 w+L\mathrm{div}\,(\Re^{-1}[\mathbf{N}](\Re\,(\mathbf{grad}(w)))=0 \qquad \text{Equ. 8}$$

We implement the Equs. 6 and 8 in a finite differences scheme.

The simulation is able to generate dynamically a pattern of fingerprints as shown in Fig. 2A and 2B, see also Video 1.

This scheme was actually designed to generate fingerprints for benchmarking biometric sensors, because it is generally illegal to collect fingerprint samples at random from individuals.

Now one may wonder whether real fingerprints can be matched. For biometric or forensic purposes, the morphological information in the fingerprints is reduced to a vector of minutiae (15). These minutiae correspond to disclinations in the pattern of ridges. In order to generate a realistic fingerprint, one can impose the position of disclinations, by fixing the vector **n** of the disclinations locally at the positions of the desired minutiae (Fig. 3). The vector (n_1, n_2) being fixed at specific points the Q-tensor is diffused in space following Equ. 6, such that eventually, the spatial variation of Q fits exactly the position and orientation of all the imposed disclinations. The shape of the deformation field is imposed around these spots so that it matches a disclination in the ridge pattern (the local shape of the field is extracted from one other spontaneous disclination in the simulation). This gives such patterns as Fig. 4. Fig. 4Top gives the real fingerprint and the distribution of imposed minutiae, Fig 4Bottom gives the pattern of Q-tensor (the vectors represent the orientation of higher eigenvalue), the corresponding ridge pattern generated by buckling the plate with the stress pattern imposed by Q, and the synthetic fingerprint. Fig. 5 shows synthetic fingerprints having the same minutiae as a real fingerprint, but with a somewhat different ridge pattern (loop or whorl, Fig. 5A) depending on the choice of parameters in the diffusion of the Q-tensor. Arch or tented patterns can also be fitted (Fig. 5B).

In conclusion, we have proposed a simple scheme to couple thin plate flexure and in-plane orientational order. The Q-tensor, which is generally viewed as an orientational order parameter, can be also viewed as an active stress source. It is actually the case that cells are aligned along the direction of their actin cortex, therefore, cells exert a stress congruent with their polarity (16). Therefore a Q-tensor formed for the purpose of describing orientation, can also be used to describe the active physical stress exerted by the cells. While the

orientation of the force is congruent with the orientation of the cell itself, the magnitude of the eigenvalues of the Q-tensor need not be identical for the parameters driving the alignment and for the parameters driving the force actuation. Only the eigenvectors should be the same. The model generates very simply typical folds such as convoluted ridges.

In the model presented here, the curvature would feedback onto the orientational order through the bending term in the energy, however the simulation of Q presented here is 2D, so curvature is absent. In the future we will add the effect of curvature by modifying the differential operators accordingly. Also, in this simulation, the plate elasticity is uniform; only the stress is anisotropic locally. The eigenvectors of principle stress could also be used to introduce a biaxial anisotropy of the elastic parameters (as for example in Ref. 14).

While biological tissue is a very complex matter, the scheme presented here is able to generate typical fingerprints with identical minutiae located at the same positions as seen on actual fingers, by hooking the orientation of the Q-tensor, and the local pattern of disclinations at the positions of minutiae.

Recently, organogenesis based on Q-tensor dynamics and elastic buckling has been proposed (17), and treating tissue as a crystal liquid has become commonplace (18). However, the data presented here were in part already presented in (19), but at the time the algorithm used was confidential and it could only be eluded without technical detail (20).

Acknowledgement. One set of data was prepared by the undergraduate student Zineb Layachi.

Legal statement : The real fingerprints have been blurred in order to comply with legal regulations.

References

1. V. Fleury, N. Chevalier, F. Furfaro, J.-L. Duband, *Eur. Phys. J. E* **38** (6), 1-19 (2015).
2. N. Tipping and D. Wilson, *Anat. Rec.* (Hoboken) **294**, 1143 (2011
3. J. L. Krans, The Sliding Filament Theory of Muscle Contraction, Nature Education **3** (9):66 (2010)
4 V. Fleury, A. V. Murukutla, *Eur. Phys. J. E* **42**, 104 (2019) doi:10.1140/epje/i2019-11869-8.
5. V. Fleury, A. V. Murukutla, A., N. Chevalier, B. Gallois, B., M. Capellazzi-Resta, P. Picquet, Peaucelle, *Phys. Rev. E* **94**, 022426 (2016).
6. V. Fleury, V., A. Abourachid, A biaxial tensional model for early vertebrate morphogenesis. *Eur. Phys. J. E* **45**, 31 (2022). https://doi.org/10.1140/epje/s10189-022-00184-4
7. N. R. Chevalier, N. Dacher, C. Jacques, L. Langlois, C. Guedj, O. Faklaris, Embryogenesis of the Peristaltic Reflex, insights into the myogenic to neurogenic transition of gut motility, *Journal of Physiology* **597** (10) 2785-2801 (2019).
8. H. G. Yevick, G. Duclos, I. Bonnet, and P. Silberzan , Architecture and migration of an epithelium on a cylindrical wire, *PNAS* **112** (19) 5944-59 (2015).
9. G. Duclos, C. Blanch-Mercader, V. Yashunsky, V. *et al.* Spontaneous shear flow in confined cellular nematics. *Nature Phys* **14**, 728–732 (2018). https://doi.org/10.1038/s41567-018-0099-7
10. P. Oswald and P. Pieranski, *Crystal liquids*, Eyrolles, Paris 2000.
11. M. Kuecken and A. Newell, A model for fingerprint formation, *Eur. Phys. Letters* **68** (1), 141-146 (2004).
12. J. D. Glover, Z. R. Sudderick, B. Bo-Ju Shih, Y. Chen, M. L. Crichton, D. J. Headon, The developmental basis of fingerprint pattern formation and variation, *Cell* **186**, 1-17 (2023)

13. V. I. Istratescu, *Fixed Point Theory: An Introduction*, (Kluwer Academic Publishers, 2001).
14. V. Fleury and T. Watanabe, Morphogenesis of fingers and branched organs: how collagen and fibroblasts break the symmetry of growing biological tissue C. R. Acad. Sci., (série biologies) **325**, 571-583, (2002).
15. R. Bansal, P. Priti Sehgal and B. Punam, Minutiae Extraction from Fingerprint Images - a Review, International Journal of Computer Science Issues **8** (5), 3, (2011).
16. J. P. Campanale , T. Y. Sun and D. J. Montell, Development and dynamics of cell polarity at a glance, *J. Cell Sci.* **130** (7): 1201–1207 (2017). doi: 10.1242/jcs.188599
17. D. Khoromskaia, G. Salbreux, Active morphogenesis of patterned epithelial shells, *eLife* **12**:e75878. (2023) https://doi.org/10.7554/eLife.75878
18. A. Doostmohammadi, B. Ladoux, Physics of liquid crystals in cell biology, *Trends in Cell Biology* **32**, 140-150, 2022. doi: 10.1016/j.tcb.2022.01.010.
19. C. Barral, Biometrics and Security: Combining Fingerprints, Smart Cards and Cryptography, PhD thesis EPFL press 2010. https://infoscience.epfl.ch/record/148685 Last access March 2023.
20. V. Fleury, Je la revois, *remue.net* (Octobre 2016).

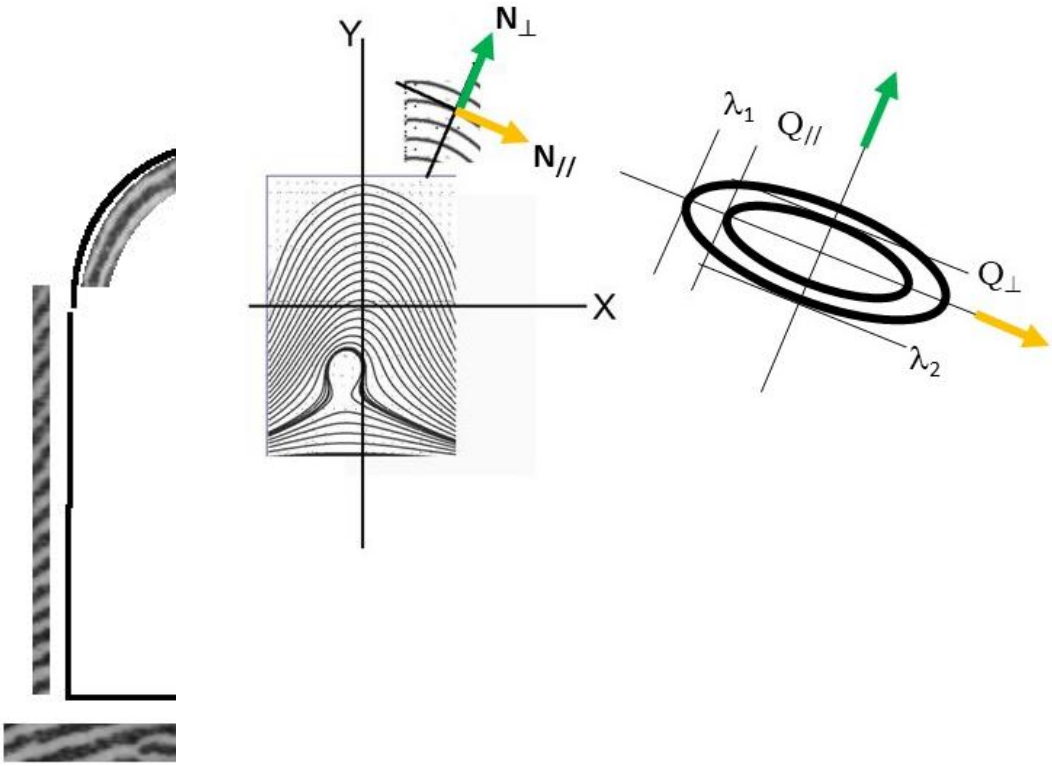

Figure 1B

Figure 1 Fig. 1A The nematoïd pattern (left) is used as stress field. Locally, the eigenvectors of the orientation Q -tensor are used to form the principal axis of the stress tensor **N** (top, vectors $\mathbf{N}_{//}$ and $\mathbf{N}_\perp$. The stress tensor and the Q-tensor have the same eigenvectors, but different eigenvalues (to the

right the ellipsoids schematize the situation: the orientations are identical, but the eigenvalues are different). The principle axis of stress will be point by point aligned with the nematoïd field, so that a pattern of ridges will be formed matching closely the given nematoïd field. Fig. 1B. The boundary conditions use the anatomical fact that the lines are aligned with the edge of the finger at the tip of the finger, with the joint of the phalanx at the first joint, and they leave the palmar side of the finger perpendicularly to the finger axis. The eigenvectors are imposed in these areas.

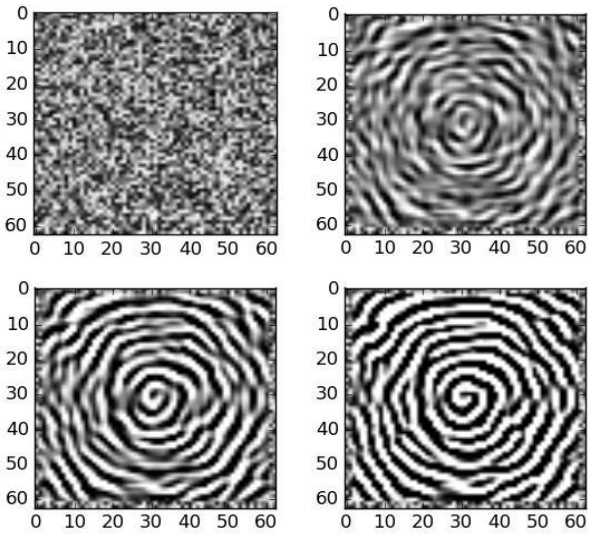

Figure 2A

Figure 2B

Figure 2 Fig. 2A Snapshots of fingerprint formation, extracted from video 1, following the buckling Equation [8], the initial configuration is some noise. The simulation runs the von Karman equation, with the nematoïd field given by the Q-tensor (here a nematoïd field with a central whorl-defect). Fig. 2B A typical fingerprint formed in our simulation, after cropping the image to give it a realistic rendering.

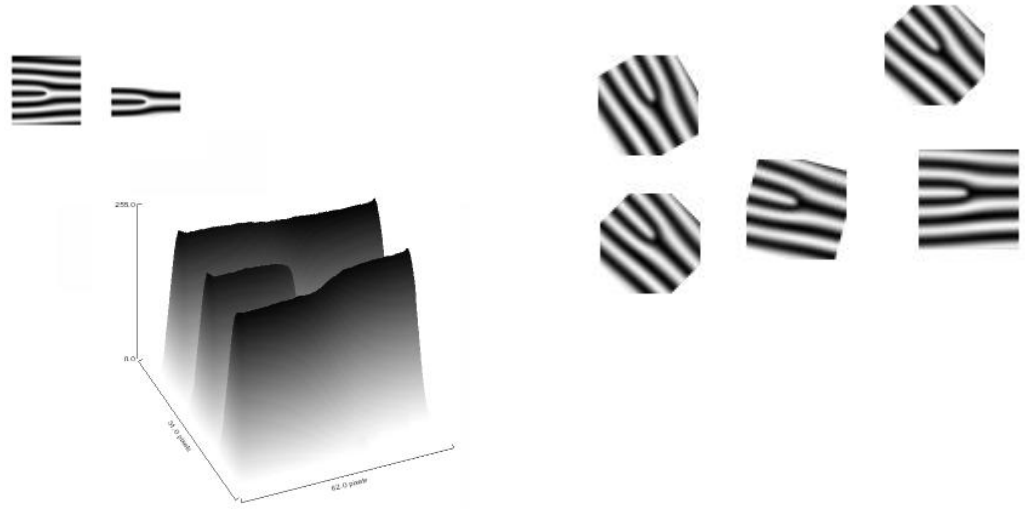

Figure 3

Figure 3 Minutiae are disclinations, which can be locally modelled by forcing a disclination in the field of orientation, and in the field of heights (Left). By orienting the local prepattern along many disclinations (Right), one can force the pattern to spouse the orientation and the disclinations locally, at will. Locally the orientation of the disclination will impose the values of the Q tensor, and a pattern having at least all these minutiae will be formed. (In practice the field around a disclination is generated by extracting a small map of heights around a disclination generated spontaneously by the simulation, in order to have the proper wavelength and the proper local variations of heights).

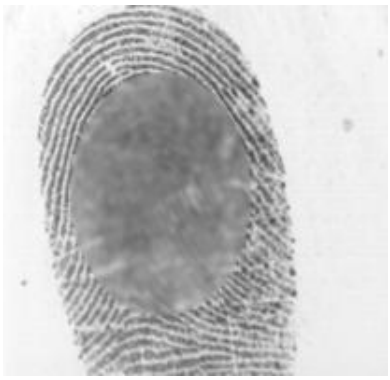

Real fingerprint

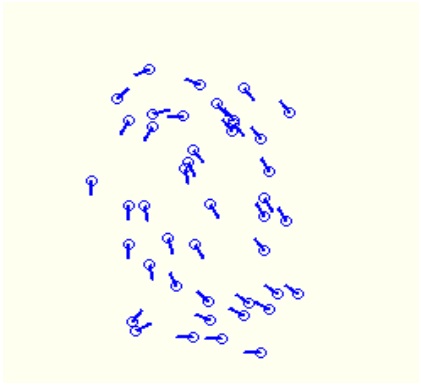

Minutiae of real fingerprint

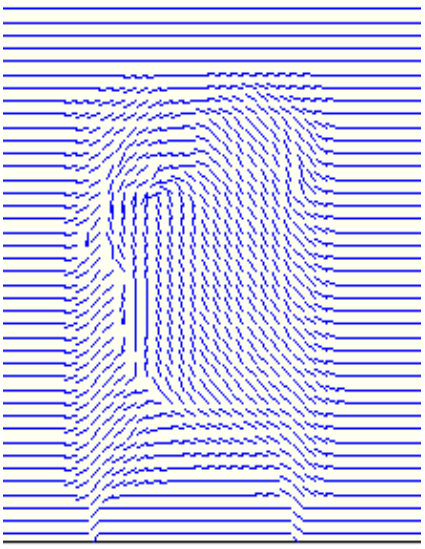

Principal axis of stress

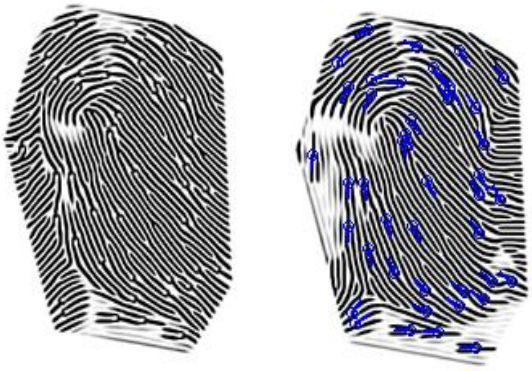

Synthetic fingerprint Minutiae of synthetic fingerprint

Figure 4 Formation of a synthetic fingerprint having disclinations located exactly at the position of known minutiae. Top, to the left the real fingerprint. To the top right position of the real minutiae. Bottom left, the Q-tensor map, then the synthetic fingerprint, then the position of the minutiae. Real fingerprints are blurred to comply with legal regulations.

Real fingerprint Synthetic fingerprints

Figure 5A

Real Fingerprint **Synthetic fingerprint**

Figure 5B

Figure 5 Figure 5A By varying the parameters in the Q-tensor dynamics or the convergence time, one can fit the same minutiae of a real fingerprint (Top left) to either a whorl pattern (Top middle) or a loop pattern (Top right) of fingerprint. (The fingerprints contrasts were treated for biometric usage). Other minutiae than the ones which are “forced” are also obtained. **Figure 5B** Arch patterns can also be fitted. Real fingerprints are blurred to comply with legal regulations.